

SCIENTIFIC REPORTS



OPEN

Pan-neurexin perturbation results in compromised synapse stability and a reduction in readily releasable synaptic vesicle pool size

Dylan P. Quinn^{1,2}, Annette Kolar^{1,2}, Michael Wigerius³, Rachel N. Gomm-Kolisko⁴, Hanine Atwi⁵, James P. Fawcett³ & Stefan R. Krueger^{1,2}

Received: 05 October 2016

Accepted: 16 January 2017

Published: 21 February 2017

Neurexins are a diverse family of cell adhesion molecules that localize to presynaptic specializations of CNS neurons. Heterologous expression of neurexins in non-neuronal cells leads to the recruitment of postsynaptic proteins in contacting dendrites of co-cultured neurons, implicating neurexins in synapse formation. However, isoform-specific knockouts of either all α - or all β -neurexins show defects in synaptic transmission but an unaltered density of glutamatergic synapses, a finding that argues against an essential function of neurexins in synaptogenesis. To address the role of neurexin in synapse formation and function, we disrupted the function of all α - and β -neurexins in cultured hippocampal neurons by shRNA knockdown or by overexpressing a neurexin mutant that is unable to bind to postsynaptic neurexin ligands. We show that neurexin perturbation results in an attenuation of neurotransmitter release that is in large part due to a reduction in the number of readily releasable synaptic vesicles. We also find that neurexin perturbation fails to alter the ability of neurons to form synapses, but rather leads to more frequent synapse elimination. These experiments suggest that neurexins are dispensable for the formation of initial synaptic contacts, but play an essential role in the stabilization and functional maturation of synapses.

Neuronal circuit development is an intricate process that culminates in the maturation of specific synaptic contacts between functionally diverse pre- and postsynaptic neurons. The mature state is preceded by a highly dynamic stage of synapse refinement during which new synaptic contacts are formed at an increased rate while inappropriate synapses are weakened and eliminated. This developmental program fine-tunes neuronal circuits in an activity-dependent manner^{1–3}. Cell adhesion proteins provide trans-synaptic contacts and are well suited to mediate synapse formation and plasticity^{4–8}. Furthermore, mutations in genes encoding synaptic adhesion proteins have been linked to neurodevelopmental disorders^{9–14}, suggesting a role of these gene products in synaptic refinement.

Neurexins (Nrxns) represent one family of structurally diverse presynaptic cell adhesion molecules that have been implicated in the structural and functional development of synapses. Nrxns bind transsynaptically to postsynaptic adhesion molecules of the neuroligin and LRRTM families as well as to GluR Δ 2/cerebellin and calstentenin-3^{15–19}. They are expressed from three different genes (Nrxn1, Nrxn2, and Nrxn3) employing two promoters in each gene²⁰. The resulting longer α -Nrxn and the shorter β -Nrxn differ in their binding affinities for postsynaptic ligands, which is further modulated by alternative splicing^{19,21}.

Initial studies indicated that Nrxns and Nrxn ligands have an important role in the formation of synapses by transsynaptically recruiting proteins to pre- and postsynaptic compartments. Thus, heterologous expression of Nrxn in non-neuronal cells elicited the accumulation of postsynaptic density proteins in dendrites at contact sites²². Similarly, expression of Nrxn ligands in non-neuronal cells resulted in the clustering of presynaptic active

¹Department of Physiology & Biophysics, Dalhousie University, Halifax Nova Scotia B3H 1X6, Canada. ²Department of Neuroscience Institute, Dalhousie University, Halifax Nova Scotia B3H 1X6, Canada. ³Department of Pharmacology, Dalhousie University, Halifax Nova Scotia B3H 1X6, Canada. ⁴Department of Psychology and Neuroscience, Dalhousie University, Halifax Nova Scotia B3H 1X6, Canada. ⁵Department of Biology, Dalhousie University, Halifax Nova Scotia B3H 1X6, Canada. Correspondence and requests for materials should be addressed to S.R.K. (email: stefan.krueger@dal.ca)

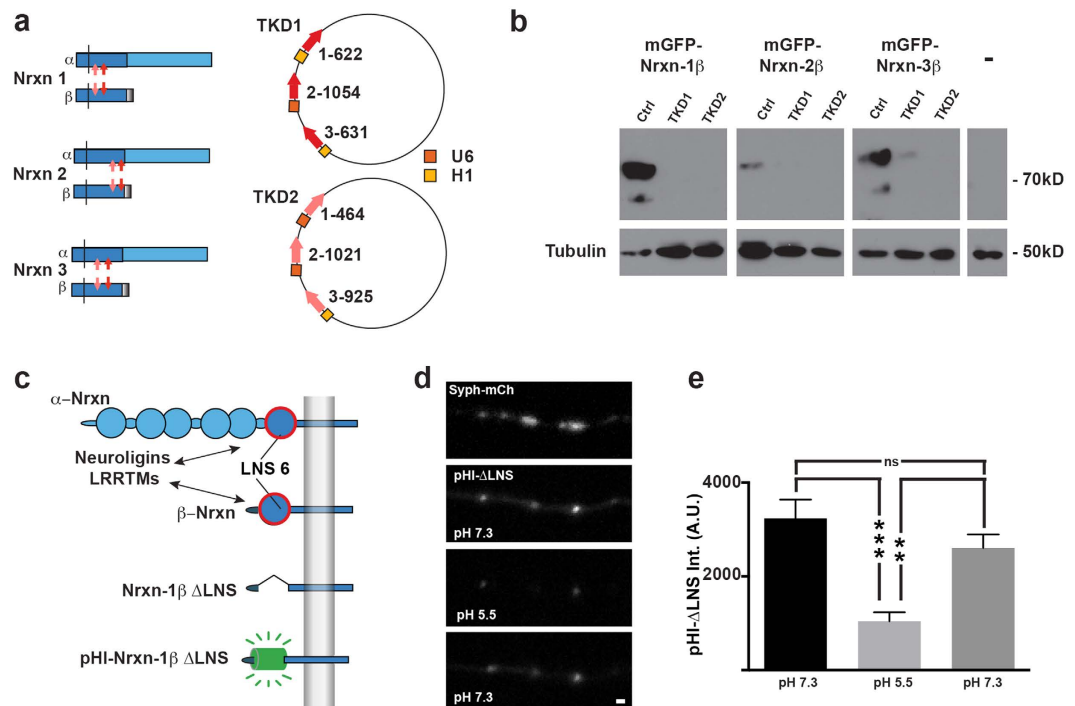


Figure 1. Molecular tools for disrupting Nrnx function. (a) For each of the 3 Nrnx gene transcripts, shRNA knockdown constructs were designed to target sequences present in both α and β Nrnx mRNA. Two different shRNA sequences were validated for each of the 3 Nrnx genes (pink and red arrows). shRNA sequences were combined into 2 unique Nrnx triple knockdown vectors (TKD1, TKD2). shRNA sequences for each TKD were driven by a combination of U6 and H1 promoters. (b) Knockdown efficiency was assessed by co-transfecting mGFP tagged versions of Nrnx 1 β , 2 β , and 3 β along with Ctrl, TKD1 or TKD2 plasmids into HEK293 cells and performing a western blot with and an anti-GFP antibody. (c) A dominant negative Nrnx-1 β construct was created by excising the extracellular LNS 6 domain of Nrnx-1 β . The LNS 6 domain is essential for the binding of Nrnx with postsynaptic Neuroligins and LRRTMs. Nrnx-1 β Δ LNS reduces Nrnx-mediated transsynaptic cell adhesion by competing with endogenous α - and β -Nrnx for binding presynaptic scaffolding proteins. We analyzed the cellular properties of Nrnx-1 β Δ LNS by tagging it to a pH sensitive fluorescent molecule called pHIuorin to create pHI-Nrxn-1 β Δ LNS. (d) Representative image of pHI-Nrxn-1 β Δ LNS (pHI- Δ LNS) construct co-transfected with Synaptophysin-mCherry (Syph-mCh). Co-localization of pHI- Δ LNS with Syph-mCh suggests that pHI- Δ LNS localizes to synapses. pHI- Δ LNS fluorescence reversibly quenches when imaged in a pH 5.5 buffer suggesting that pHI- Δ LNS is properly inserted into the plasma membrane. (e) Average fluorescent intensity of pHI- Δ LNS puncta was significantly reduced by imaging in pH 5.5 buffer and recued upon perfusion of original pH 7.3 imaging buffer. ** $p < 0.01$, and *** $p < 0.001$ as determined by 1-way ANOVA and post hoc Tukey test. $N = 34$ pHI- Δ LNS puncta. Scale bar = 1 μ m.

zone material within contacting axons^{16,18,19,23}. Investigations into the function of Nrnxns have also been aided by knockout studies in which specific Nrnx isoforms or Nrnxns ligands were targeted. Deletion of either all 3 α -Nrnxns²⁴ or all 3 β -Nrnxns²⁵ resulted in an impairment of neurotransmission at glutamatergic synapses that was at least partly due to a reduction in neurotransmitter release. Surprisingly, however, the density of glutamatergic synapses in both α - and β -Nrnxn-deficient mouse models was found to be unchanged^{24,25}. Similarly, deletion or knockdown of individual or multiple postsynaptic Nrnx ligands resulted in attenuated neurotransmission, but failed to affect synapse density^{26,27} (but see²⁸). Collectively, these findings conflict with a proposed role of Nrnxns in synaptogenesis. It is important to note, however, that in the aforementioned studies, transsynaptic adhesion between Nrnxns and their postsynaptic ligands was only partially disrupted. In the mammalian CNS, Nrnxns and Nrnxn ligands are expressed in a highly redundant, albeit cell type-specific, manner in individual neurons^{19,26,29-31}. It therefore remains possible that the remaining isoforms in these mouse models were fully sufficient to support a permissive function of Nrnxns in synaptogenesis.

In this study, we address the role of Nrnxns in synapse formation by interfering with the function of all Nrnx isoforms using two independent approaches. Our data reveal that a pan-Nrnx perturbation has profound consequences for the stabilization and functional maturation of synaptic contacts.

Results

Molecular tools for disrupting the function of all Nrnx isoforms. To disrupt the function of all α - and β -Nrnxns, we took two approaches. First, we designed Nrnx shRNA constructs that targeted each of the 6 primary Nrnx mRNA transcripts (Fig. 1a). shRNA constructs were designed to target mRNA sequences present

in both α and β Nrnx transcripts so that a single shRNA should attenuate expression of both α and β isoforms for a particular Nrnx gene. The effectiveness of individual shRNA in reducing exogenous neurexin mRNA was first screened in a fluorescent assay in neurons (Supplemental Fig. S1). Effective shRNAs were then combined into two triple knockdown vectors (TKD1 and TKD2), each with unique shRNA sequences target towards Nrnx 1, 2, and 3 mRNA (Fig. 1a, right). Neurexin TKD1 and TKD2 constructs were further evaluated by co-transfecting mGFP fusion-tagged constructs of Nrnx 1 β , 2 β , and 3 β along with Ctrl, TKD1 or TKD2 plasmids into HEK293 cells and performing a western blot with an anti-GFP antibody (Fig. 1b; for original Western blots see Supplemental Fig. S2).

In a second approach to disrupt the function of all Nrnxns, we created a mutant Nrnx-1 β construct in which the LNS domain essential for binding neuroligins and LRRTMs was deleted (Nrnx-1 β Δ LNS, Fig. 1c). To characterize the subcellular localization of Nrnx-1 β Δ LNS, we inserted the pH-sensitive fluorescent protein, supercliptic pHluorin (pHl) in place of the extracellular LNS domain to create pHl-Nrnx-1 β Δ LNS (pHl- Δ LNS, Fig. 1c–e). pHl- Δ LNS co-localized with synaptophysin-mCherry (Syph-mCh) puncta at putative presynaptic specializations (Fig. 1d). To test whether the pHl- Δ LNS construct was properly inserted into the plasma membrane, we imaged pHl- Δ LNS expressing axons before, during, and after perfusion with a pH 5.5 buffer. The average fluorescent intensity of pHl- Δ LNS puncta was significantly reduced during perfusion of the pH 5.5 buffer and increased upon reperfusion with pH 7.3 buffer (Fig. 1e. ** $p < 0.01$, and *** $p < 0.001$ as determined by 1-way ANOVA and post hoc Tukey test). Taken together, these findings suggest that the pHl- Δ LNS construct is correctly inserted into the plasma membrane at presynaptic specializations.

To confirm that knockdown and Nrnx-1 β Δ LNS constructs perturb the function of endogenous neurexins in neurons, we co-cultured neurons transfected with knockdown or Nrnx-1 β Δ LNS constructs with fibroblasts expressing the neurexin ligand LRRTM2. Non-neuronally expressed LRRTM2 induces the recruitment of presynaptic specializations, or hemisynapses, in contacting axons in a neurexin-dependent manner^{16,32}. Functional perturbation of endogenous neurexins should inhibit the formation of hemisynapses at contact sites with LRRTM2 expressing fibroblasts. We co-cultured COS7 cells with dissociated hippocampal neurons that were transfected with either an empty knockdown vector (pS), NrnxTKD1, NrnxTKD2 or Nrnx-1 β Δ LNS. Synaptophysin-mCherry (Syph-mCh) was included in the neuronal transfection as a fluorescent marker of synaptic vesicles to detect hemisynapses. After 48 hours, co-cultures were fixed and neuronal dendrites were immunostained with an antibody raised against MAP2 to exclude Syph-mCh puncta made onto dendrites from the analysis. LRRTM2-CFP expression in COS7 cells induced dramatic clustering of Syph-mCh puncta in control axons expressing an empty knockdown vector, in contrast to COS cells expressing a CFP control vector (Fig. 2a). Compared to control axons, expression of NrnxTKD1, NrnxTKD2 or Nrnx-1 β Δ LNS in neurons significantly reduced both the average number of Syph-mCh puncta per COS7 cell (Fig. 2b1, * $p < 0.05$, ** $p < 0.01$, one-way ANOVA and post hoc Tukey test), as well as the average intensity of Syph-mCh puncta per COS7 cell (Fig. 2b2, $p < 0.01$, one-way ANOVA and post hoc Tukey test). These data suggest that shRNA constructs diminish endogenous Nrnx expression and that our Nrnx-1 β Δ LNS acts in a dominant negative fashion to perturb Nrnx function, presumably by inhibiting the binding of endogenous α - and β -Nrnxns to presynaptic scaffolding proteins such as the CASK/Mint1/Veli complex^{33,34}.

Perturbation of Nrnx function reduces readily releasable pool size and attenuates neurotransmitter release probability. Electrophysiological studies of Nrnx gene knockouts have indicated isoform-specific roles of Nrnxns in the modulation of neurotransmitter release^{24,25}. In contrast, several studies that have disrupted the function of one or several postsynaptic Nrnx ligands have failed to find evidence for changes in presynaptic function^{27,35,36}, questioning the notion of a transsynaptic modulation of neurotransmitter release through postsynaptic Nrnx ligands³⁷. To test the role of Nrnxns in the modulation of neurotransmitter release, we used a genetically encoded sensor, synaptophysin-pHluorin (Syphl), to quantify synaptic vesicle exocytosis at synapses from neurons with attenuated Nrnx function. In comparison to electrophysiological recordings, this optical method has the advantage of probing presynaptic function directly, in isolation from any effects of Nrnx perturbation on synaptic density and the recruitment of postsynaptic neurotransmitter receptors.

Cultures of dissociated hippocampal cells were transfected at 12–14 DIV with either Nrnx knockdown or Nrnx-1 β Δ LNS plasmids or a knockdown vector devoid of shRNA sequences, along with Syphl. Synaptophysin-mCherry (Syph-mCh) was included in the transfection mixes and was used to identify transfected axons (Fig. 3a, top panel). A high-frequency stimulus train (80 Hz for 1 s) was used to compare the size of the readily releasable pool (RRP) of synaptic vesicles at synapses from neurons expressing NrnxTKD1, Nrnx-1 β Δ LNS or empty knockdown vector (Fig. 3a, middle panel; Fig. 3b, upper graph). The Syphl fluorescence increase in response to high-frequency train stimulation, $\Delta F(80 \text{ Hz}, 1 \text{ s})$, was reduced by 34% and 32% in NrnxTKD1 and Nrnx-1 β Δ LNS groups, respectively, compared to control cultures (Fig. 3c, upper graph), indicating a reduction of RRP size in both groups ($p < 0.01$, one-way ANOVA and post hoc Tukey test). To ensure that the effects of NrnxTKD1 shRNA on RRP size are not due to off-target effects of the shRNA, we performed a separate set of experiments using NrnxTKD2, a KD plasmid with 3 different shRNA sequences targeted towards Nrnx mRNA. Perturbation of Nrnx function with NrnxTKD2 resulted in a comparable reduction in peak Syphl fluorescence during high frequency stimulation (41% reduction, $p < 0.001$, Student's t-test, independent samples, Fig. 3c, lower graph). At synapses that responded to high frequency stimulation, we measured the Syphl fluorescence increases in response to single action potentials, $\Delta F(1 \text{ AP})$, a measure of the probability of neurotransmitter release at individual presynaptic specializations (Pr^{38}). Average Syphl fluorescence increases in response to isolated action potentials were strongly reduced in NrnxTKD1 and Nrnx-1 β Δ LNS groups (Fig. 3d). Compared to control synapses, $\Delta F(1 \text{ AP})$ was reduced by 81% at NrnxTKD1 synapses and 66% at Nrnx-1 β Δ LNS synapses (** $p < 0.01$, *** $p < 0.001$, one-way ANOVA and post hoc Tukey test).

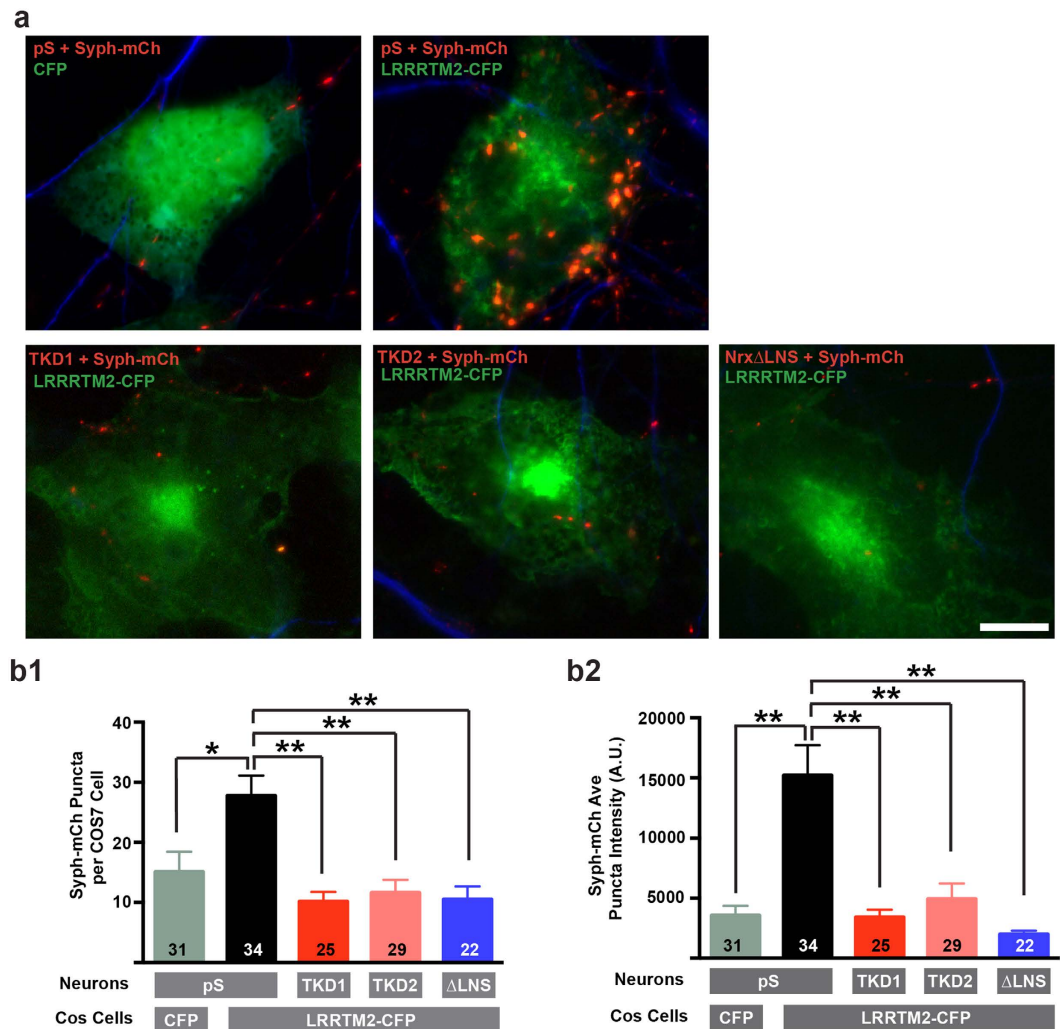


Figure 2. Perturbation of Nrnx function blocks the synaptogenic effect of LRRTM2 in co-culture synapse formation assay. (a) COS7 cells expressing CFP or LRRTM2-CFP cultured with hippocampal neurons expressing either an empty knockdown vector (pS), NrnxTKD1, NrnxTKD2, or Nrnx-1 β ΔLNS along with Synaptophysin-mCherry (Syph-mCh, red). CFP in COS7 cells is pseudo-colored green to allow for better detection of anti-MAP2 stained dendrites, shown in blue. (b) Quantification of Syph-mCh puncta density and intensity. LRRTM2-induced clustering of Syph-mCh puncta in NrnxTKD1, NrnxTKD2, or Nrnx-1 β ΔLNS expressing axons was significantly reduced compared to axons expressing an empty knockdown vector when quantified as average number of Syph-mCh puncta per COS7 cell (b1) or as average Syph-mCh cluster intensity per COS7 cell (b2; * $p < 0.05$, ** $p < 0.01$, as determined by 1-way ANOVA and post hoc Tukey test). Numbers of COS7 cells analyzed are indicated in the graphs. Data are shown as mean \pm SEM. Scale bar indicates 10 μ m.

While the amplitude of SypHl fluorescence increases to high-frequency train stimulation allows an assessment of RRP size, the density of axonal varicosities with increases in SypHl fluorescence can serve as a measure of the density of synapses that release neurotransmitter. We therefore also analyzed the effect of Nrnx perturbation on the density of axonal sites with SypHl fluorescence increases in response to high frequency stimulation. Neurons expressing NrnxTKD1 and Nrnx-1 β ΔLNS groups showed a 73% and 56% reduction, respectively, in the density of axonal sites displaying a SypHl fluorescence increase in response to high-frequency stimulation as compared to control neurons expressing the knockdown vector lacking the shRNA ($p < 0.01$, one-way ANOVA and post hoc Tukey test, Fig. 3e, upper graph). Similarly, neurons expressing NrnxTKD2 displayed 49% reduction in the density of axonal sites with SypHl increases ($p < 0.001$, Student's t-test for independent samples, Fig. 3e, lower graph). Taken together, these results suggest that disruption of Nrnx function causes a decrease in release probability that is partly due to a reduction in RRP size, as well as a reduction in the density of functional synapses.

Nrnx disruption reduces active zone protein content and synaptic density. As outlined above (Fig. 3), disruption of Nrnx function causes a reduction in the size of the readily releasable pool (RRP) of synaptic vesicles. It has previously been shown that RRP size correlates with the size of the active zone cytomatrix^{38,39}, which presumably determines the number of docking sites available for synaptic vesicles. We therefore tested

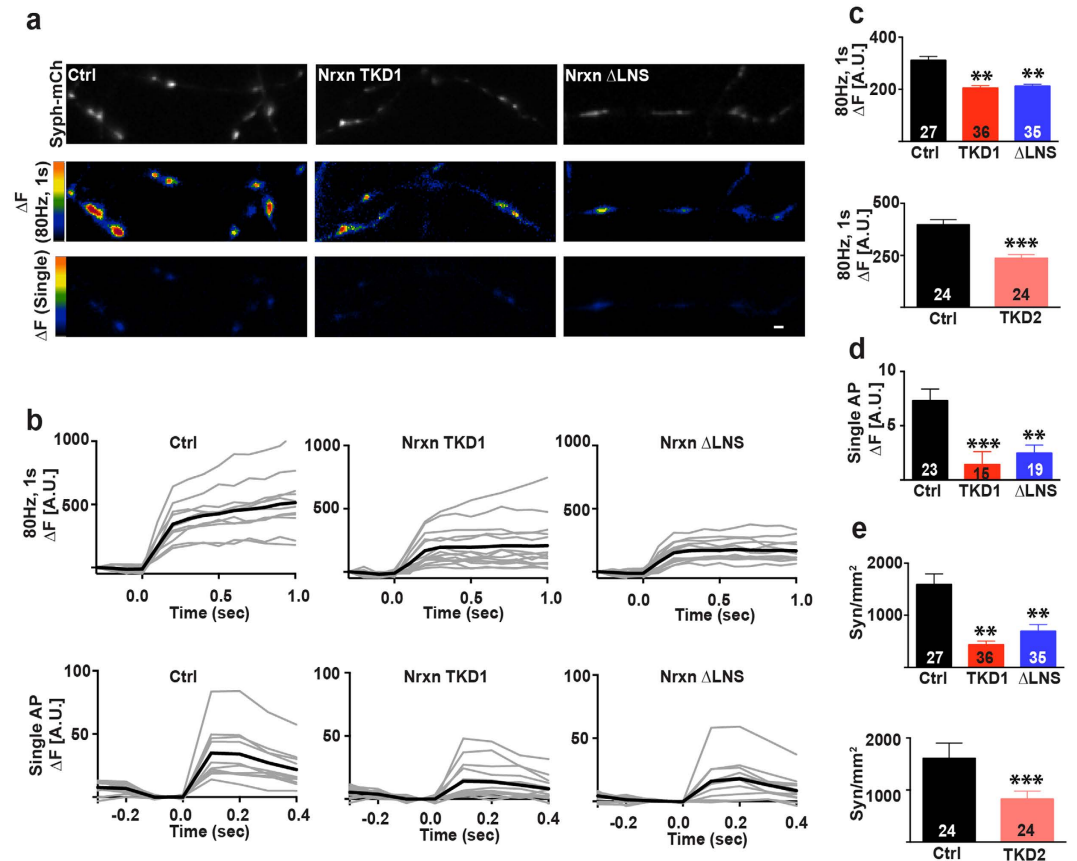


Figure 3. Nrnx perturbation attenuates neurotransmitter release. (a) Upper panel: synaptophysin-mCherry (SypH-mCh) expressing axons for control, NrnxTKD1 and Nrnx-1 β ΔLNS groups. SypH-mCh puncta were used to identify transfected axons. Middle Panel: SypHl fluorescence change (ΔF) that occurs during high frequency stimulation, ΔF (80 Hz, 1 s), which exhausts the readily releasable pool of synaptic vesicles. Lower panel SypHl fluorescence change that occurs during single stimulation (ΔF (Single)). (b) SypHl fluorescent traces for micrographs presented above. Upper panel: SypHl fluorescence traces during high frequency stimulation (ΔF (80 Hz, 1 s)) for control, NrnxTKD1 and Nrnx-1 β ΔLNS groups. Lower panel: SypHl fluorescence traces during single stimulation (ΔF (Single)) for control, NrnxTKD1 and Nrnx-1 β ΔLNS groups. Gray traces show SypHl ΔF at individual synapses (high frequency stimulation averaged over 4 trials; single stimulation averaged over 180 trials). Black traces show the average synaptic SypHl response. (c) Average SypHl fluorescence changes per experiment in response to high frequency stimulation for NrnxTKD1/Nrnx-1 β ΔLNS experiments (upper graph) and for NrnxTKD2 experiments (lower graph). (d) Average SypHl fluorescence changes per experiment in response to single stimulation for NrnxTKD1/Nrnx-1 β ΔLNS experiments. (e) Density of high frequency SypHl fluorescent responses for NrnxTKD1/Nrnx-1 β ΔLNS experiments (upper graph) and for NrnxTKD2 experiments (lower graph). ** $p < 0.01$ and *** $p < 0.001$ as determined by 1-way ANOVA and post hoc Tukey test. Data are shown as mean \pm SEM. Number of independent experiments are indicated in the respective graphs. Number of analyzed puncta = 1919, 697, and 1086 for Ctrl, NrnxTKD1, and Nrnx-1 β ΔLNS respectively in the upper panels of Fig. 3c and e. Number of analyzed puncta = 1727 and 887 for Ctrl and NrnxTKD2 respectively in the lower panels of Fig. 3c and e. Number of analyzed puncta = 1116, 297, and 502 for Ctrl, NrnxTKD1, and Nrnx-1 β ΔLNS respectively in Fig. 3d. Scale bar = 1 μ m.

if perturbation of Nrnx function alters the recruitment of active zone cytomatrix proteins to presynaptic specializations. For this purpose, we transfected hippocampal cultures at 12–14 DIV with either empty KD vector, NrnxTKD1, NrnxTKD2 or Nrnx-1 β ΔLNS along with a plasmid encoding synaptophysin-EGFP (SypH-EGFP) to mark transfected axons and presynaptic specializations. Three days following the transfection, we performed immunocytochemistry to quantify the amount of the active zone cytomatrix proteins Bassoon (Bsn) and, in a separate set of experiments, Rab3-associated molecule 1/2 (RIM1/2). We also immunolabeled microtubule associated protein 2 (MAP2) to restrict our analysis to points of contact between transfected axons and MAP2-positive dendrites (Fig. 4a). We observed that NrnxTKD or overexpression of Nrnx-1 β ΔLNS significantly attenuated the intensity of Bsn and RIM puncta at axodendritic contacts (Fig. 4d). Average Bsn intensity was reduced by 29.8% with NrnxTKD, 28.5% with NrnxTKD2, and 39.4% with Nrnx-1 β ΔLNS ($p < 0.01$ as determined by 1-way ANOVA and post hoc Tukey test). Average RIM intensity per experiment was reduced by 33.3% with NrnxTKD and 44% with Nrnx-1 β ΔLNS ($p < 0.01$ as determined by 1-way ANOVA and post hoc Tukey test). Histograms for Bsn and RIM puncta intensity suggest that Nrnx perturbation results in a proportional reduction of Bsn and RIM

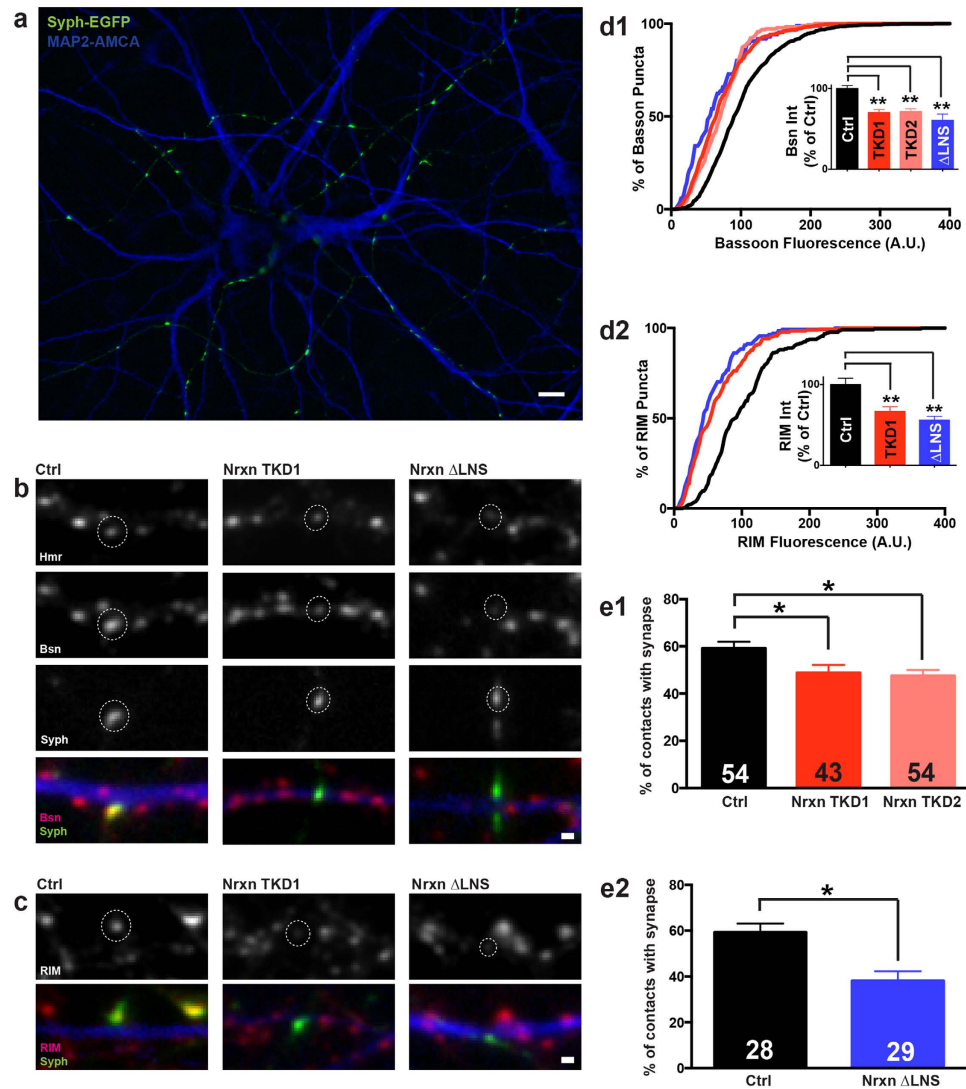


Figure 4. Nrnx disruption reduces active zone cytomatrix protein content and synaptic density.

(a) Overview image of synaptic contacts between MAP2 positive dendrites (blue) and axons co-transfected with synaptophysin-EGFP (syph-EGFP, green) + experimental treatment (Ctrl plasmid, NrnxTKD1 or Nrnx-1 β ΔLNS). (b–c) Nrnx disruption decreases immunofluorescence of active zone cytomatrix proteins. (b) Upper 3 panels: representative images of Homer and Bassoon (Bsn) immunostains and syph-EGFP expressing axons for the 3 experimental groups. Circled puncta show Bsn and Homer clusters that correspond to the transfected axon. Bottom panel: Merged image of Bsn (red), Syph-EGFP (green) and MAP2 (blue) fluorescence. (c) Upper panel: RIM1/2 immunofluorescence for the 3 experimental groups. Bottom panel: Merged image of RIM (red), Syph-EGFP (green) and MAP2 (blue) fluorescence. (d) Cumulative histogram of immunofluorescence for Bsn (d1) and RIM1/2 (d2). Inset graphs show average puncta immunofluorescence, normalized to control. For Bsn immunofluorescence experiments, n = 89, 57, 38 and 30 postsynaptic neurons for Ctrl, TKD1, TKD2, and Nrnx-1 β ΔLNS groups respectively. For RIM immunofluorescence experiments, n = 25, 23, and 21 postsynaptic neurons for Ctrl, TKD1, and Nrnx-1 β ΔLNS groups respectively. **p < 0.01 as determined by 1-way ANOVA and post hoc Tukey test. (e1–e2) Nrnx disruption reduces synaptic density. Percentage of axodendritic contacts with both Bsn and Homer clusters per experiment for NrnxTKD1 (e1) and Nrnx-1 β ΔLNS overexpression (e2). The number of analyzed postsynaptic neurons is indicated in the respective graphs. *p < 0.05 as determined by 1-way ANOVA and post hoc Tukey test (For TKD experiments) and Student's t-test (For Nrnx-1 β ΔLNS experiments). Data are shown as mean \pm SEM. Number of analyzed puncta = 894, 612, 181, and 85 for Ctrl, NrnxTKD1, NrnxTKD2 and Nrnx-1 β ΔLNS respectively in Fig. 4d1; 226, 190 and 138 for Ctrl, NrnxTKD1 and Nrnx-1 β ΔLNS respectively in Fig. 4d2; 759, 520 and 767 for Ctrl, NrnxTKD1 and NrnxTKD2 respectively in Fig. 4e1 and 636 and 708 for Ctrl and Nrnx-1 β ΔLNS respectively in Fig. 4e2. Scale bars = 10 μ m (a), 1 μ m (b–c).

at all synapses rather than a selective reduction at a subset of synapses. These results show that Nrnx is important for the recruitment of active zone cytomatrix proteins Bsn and RIM at axodendritic contacts and indicate that

the reduction in neurotransmitter release in NrnxTKD1, NrnxTKD2 and Nrnx-1 β Δ LNS expressing neurons may partly be due to alterations in active zone cytomatrix size or composition.

Our experiments using SypH1 to assess the density of functional presynaptic sites indicated that neurons with perturbed Nrnx function may have fewer synaptic contacts. To further investigate this possibility, we transfected neurons in hippocampal cultures with NrnxTKD1, NrnxTKD2 or Nrnx-1 β Δ LNS along with a plasmid encoding synaptophysin-EGFP to mark transfected axons. Since our transfection method results in sparse expression of the construct in 5–10% of all neurons, we were unable to employ the conventional methodology of measuring the density of dendritic spines in postsynaptic neurons. We therefore developed a novel approach to quantify synapse density on transfected cultures immunostained for Bsn, the postsynaptic protein Homer1, and MAP2. We initially identified points at which axons of transfected neurons traversed MAP2-positive dendrites. We then determined the fraction of contact points bearing co-localized Bsn and Homer1 puncta as a measure of the density of synaptic contacts made by transfected presynaptic neurons (Fig. 4a–c). Compared to control neurons, neurons expressing NrnxTKD1, NrnxTKD2 or Nrnx-1 β Δ LNS constructs displayed a significant reduction in the fraction of axodendritic contacts bearing synapses (Fig. 4e). In NrnxTKD experiments, the average percentage of synapse-bearing axodendritic contacts was 59.2+/-2.8% for Ctrl, 48.8+/-3.3% for NrnxTKD, and 47.6+/-2.5% for NrnxTKD2 ($p < 0.05$ as determined by 1-way ANOVA and post hoc Tukey test). In experiments assessing the effect of Nrnx-1 β Δ LNS on synaptic density, the average percentage of synapse-bearing axodendritic contacts per experiment was 59.4+/-3.7% for Ctrl and 38.2+/-4.1% for Nrnx-1 β Δ LNS ($p < 0.05$ for as determined by Student's t-test). Together, these experiments demonstrate that functional perturbation of all Nrnxns leads to a reduction in the density of glutamatergic synapses.

Nrnx disruption reduces the stability of synaptic contacts. The reduced density of glutamatergic synapses we observed at contacts between Nrnx-perturbed axons and dendrites may be either due to a reduced rate of synapse formation or, alternatively, an increased rate of synapse elimination. To discern between these two possibilities, we performed live time-lapse imaging of fluorescently labeled hippocampal neurons. We first co-transfected empty knockdown, NrnxTKD1 or Nrnx-1 β Δ LNS plasmids along with SypH-mCh to label presynaptic specializations. We then subsequently transfected PSD95-EGFP to label postsynaptic densities in a separate population of neurons. Co-localizations of SypH-mCh and PSD95-EGFP were imaged over a period of 24 hours and the percentage of stable, eliminated, and newly formed synapses was recorded in NrnxTKD1 and Nrnx-1 β Δ LNS groups and compared with control cultures. In all groups, we found examples of co-localized SypH-mCh and PSD95-EGFP that were stable, eliminated or newly formed during the observation period (Fig. 5a). Quantification of the percentage of stable, eliminated, and newly formed synaptic contacts showed that both NrnxTKD1 and Nrnx-1 β Δ LNS overexpression resulted in synaptic contacts that were significantly less stable compared to control cultures (Fig. 5b). In experiments employing NrnxTKD1 to perturb Nrnx function, the percentage of stable synapses per postsynaptic cell over 24 hours was 52.0+/-2.7% in Ctrl and 42.3+/-3.4% in NrnxTKD1 expressing axons ($p < 0.05$, Student's t-test). In separate experiments using Nrnx-1 β Δ LNS, the percentage of stable synapses per postsynaptic cell was 46.7+/-4.9% in ctrl and 27.7+/-7.0% in Nrnx-1 β Δ LNS expressing neurons ($p < 0.05$, Student's t-test). Interestingly, in both NrnxTKD1 and Nrnx-1 β Δ LNS groups, rates of synapse formation were not significantly different from those in control cultures. In summary, these experiments provide evidence for the notion that Nrnxns have an important role in the stabilization of synapses but are not essential for the formation of initial synaptic contacts.

Discussion

In this study, we show that the Nrnx family of presynaptic cell adhesion molecules play an important role in the functional and structural integrity of synaptic contacts. Disruption of Nrnx function in hippocampal neurons, either by shRNA-mediated knockdown of all Nrnx isoforms or by overexpression of a mutant Nrnx unable to bind postsynaptic ligands, led to a reduction in neurotransmitter release probability at affected synapses. The perturbation of Nrnx function also caused a reduction of the density of glutamatergic synaptic connections. Importantly, using time-lapse imaging of synaptically connected neurons, we show that disruption of Nrnx function increases the rate of synapse elimination but does not affect the rate of synaptogenesis. Our data therefore suggest a prominent function of these presynaptic cell adhesion proteins in the stabilization and functional maturation of glutamatergic synapses.

By using an optical method to directly measure synaptic vesicle exocytosis in cultured hippocampal neurons, we demonstrate that release probability is strongly reduced at synapses with attenuated Nrnx function. This finding is consistent with electrophysiological evidence from previous studies indicating that a reduction in neurotransmitter release probability at glutamatergic synapses in mice deficient in either all α - or all β -Nrnxns^{24,25}. Our results further suggest that the attenuation of neurotransmitter release probability in Nrnx-depleted neurons is in part due to a strong reduction in the size of the readily releasable pool of synaptic vesicles. The reduction in RRP size we observed with pan-Nrnx knockdown was more pronounced than the decrease in α -Nrnx specific knockout neurons²⁴ and in contrast to unchanged pools of readily releasable synaptic vesicles in β -Nrnx deficient neurons²⁵. To enter the RRP, synaptic vesicles have to dock to the plasma membrane and undergo SNARE complex formation, or priming. These processes crucially depend on the availability of active zone cytomatrix components that provide synaptic vesicle docking sites and facilitate priming. Interestingly, we show here that two components of active zone cytomatrices, Bsn and RIM, are reduced at synapses made by neurons with perturbed Nrnx function. This finding suggests that the decrease of RRP size observed with disruption of Nrnx function may be secondary to diminished recruitment of active zone cytomatrix components, which then causes a reduction in synaptic vesicle docking and priming.

With this study, we further sought to clarify the role of Nrnxns in synapse formation. Co-culture studies have shown that Nrnxns and Nrnx ligands are able to recruit components of pre- and postsynaptic specializations to

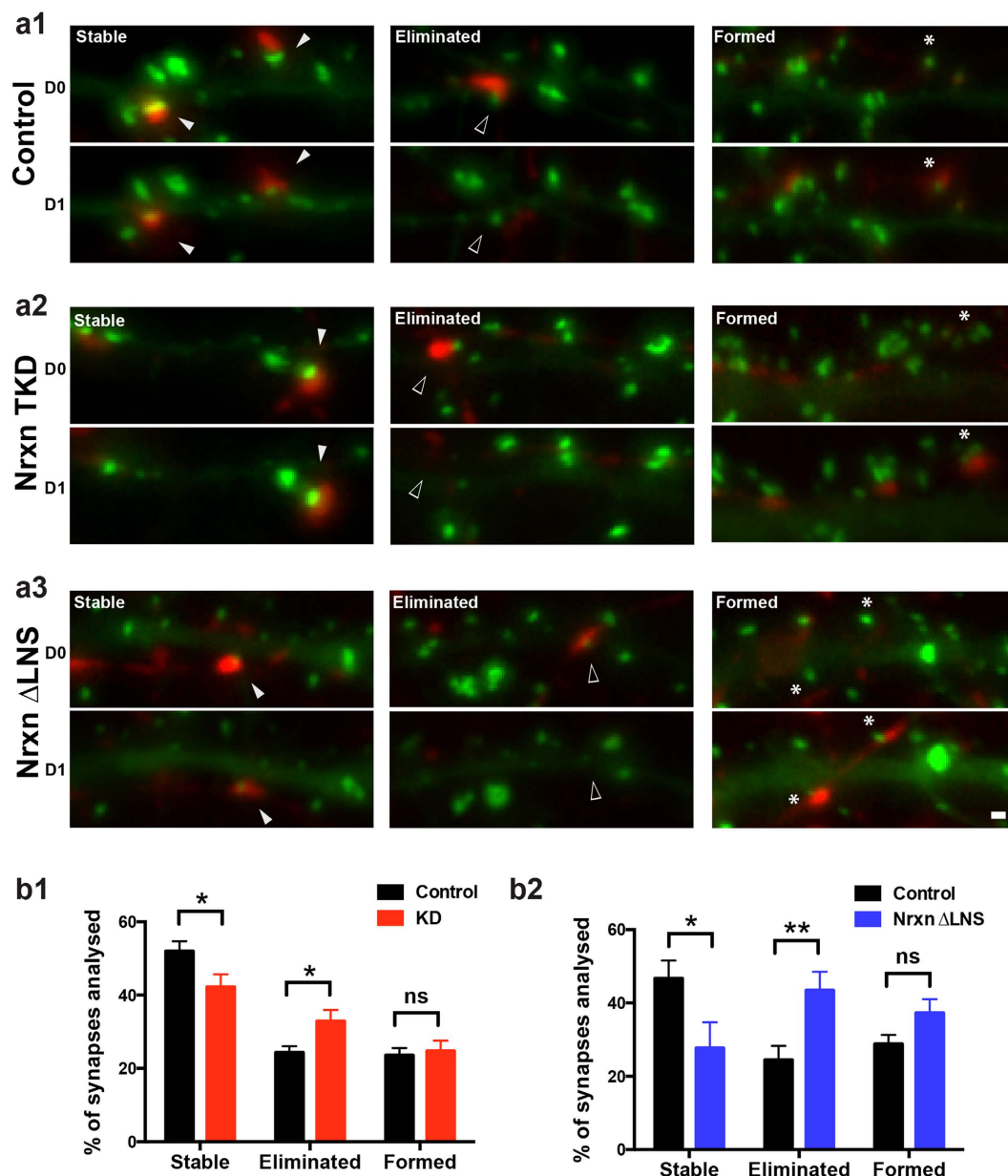


Figure 5. Nrnx disruption reduces the stability of synaptic contacts. (a1–a3) Example images of contacts between syph-mCherry expressing axons and PSD95-EGFP expressing dendrites imaged on Day 0 and 24 hrs later (Day1). Examples of stable (filled arrowheads), eliminated (open arrowheads), and formed synapses (asterisks) are shown for control, NrnxTKD1, and Nrnx-1 β Δ LNS groups. (b1–b2) Average percentage of stable, eliminated and formed synapses, grouped by postsynaptic cell for NrnxTKD1 (b1) and Nrnx-1 β Δ LNS (b2) experiments. * $p < 0.05$, ** $p < 0.01$ as determined by Student's t-test. In NrnxTKD1 experiments $n = 41$ (Ctrl) and 39 (NrnxTKD1) postsynaptic neurons. In Nrnx-1 β Δ LNS experiments, $n = 14$ (Ctrl) and 11 (Nrnx-1 β Δ LNS) postsynaptic neurons. Data are shown as mean \pm SEM. Number of analyzed synapses = 566 and 614 for Ctrl and NrnxTKD1 respectively in Fig. 5b,1 and 345 and 185 for Ctrl and Nrnx-1 β Δ LNS respectively in Fig. 5b2. Scale bar = 1 μ m.

synapses, suggesting a synaptogenic function of these proteins. However, isoform-specific knockouts of either all α - or all β -Nrnx did not lead to reductions in synaptic density, suggesting that these cell adhesion proteins are potentially dispensable for synaptogenesis^{24,25}. To examine the role of Nrnx in synaptic development, we interfered with the function of all Nrnx isoforms and assessed the effect of this manipulation on synapse density as well as on synaptic turnover. Immunocytochemical analysis of pre- and postsynaptic protein content showed that pan-Nrnx KD or overexpression of Nrnx-1 β Δ LNS results in a significant reduction in the density of glutamatergic synapses. This result is consistent with previous studies demonstrating that overexpression of neuroligins increases the density of glutamatergic synapses, while the attenuation of neuroligin and LRRTM2 expression decreases their density^{28,40}. To address whether this reduction is the result of a decreased rate of synapse

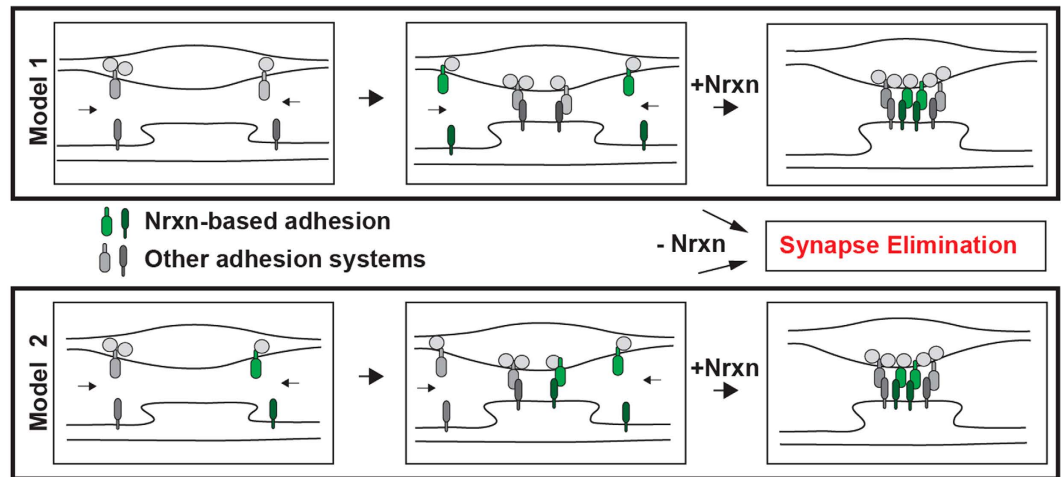


Figure 6. Model 1 (upper panel) The initial formation of synaptic contacts is mediated by synaptic cell adhesion proteins other than Nrnx. Nrnx and/or postsynaptic Nrnx ligands may be incorporated into synapses only during their maturation, and may prevent elimination of nascent synapses at this stage. Model 2 (lower panel) Nrnx are co-expressed with other cell adhesion proteins and function redundantly before the formation of synaptic contacts to induce synapse formation. Elimination of one class of adhesion molecules has little effect on the rate of synapse formation, because other cell adhesion proteins are able to fully compensate. However, the attenuation of transsynaptic cell adhesion during synaptic maturation may place synapses deficient in any individual cell adhesion protein at a disadvantage and favor their elimination.

formation or due to increased synapse elimination, we carried out time-lapse imaging of synaptically connected hippocampal neurons. Surprisingly, we found that Nrnx perturbation did not affect the rate of synapse formation but instead increased the elimination of preexisting synaptic contacts.

These results indicate that Nrnx function in the stabilization and maturation of already formed synaptic contacts and are consistent with two alternative models (Fig. 6). In the first model, the initial formation of synaptic contacts between cortical neurons is mediated by synaptic cell adhesion proteins other than Nrnx. Nrnx and/or postsynaptic Nrnx ligands may be incorporated into synapses only during their maturation, and may prevent elimination of nascent synapses at this stage. In an alternative scenario, Nrnx are co-expressed with other families of cell adhesion proteins, such as receptor protein tyrosine phosphatases, before the formation of synaptic contacts and induce synapse formation in a highly redundant manner. In this model, which is also consistent with the findings of studies showing formation of presynaptic specializations in axons contacting non-neuronal cells expressing Nrnx ligands^{16,18,19,23}; elimination of one class of cell adhesion proteins has little effect on the rate of synapse formation, because other cell adhesion proteins are able to fully compensate. However, the attenuation of transsynaptic cell adhesion during synaptic maturation may place synapses deficient in any individual cell adhesion protein at a disadvantage and favor their elimination. To conclusively distinguish between these alternative models, better insight into the role of other families of synaptic cell adhesion proteins in synapse stabilization is required.

Methods

Generation of shRNA Nrnx knockdown constructs. Short-hairpin RNA sequences were designed using software from the Whitehead Institute (<http://sirna.wi.mit.edu>). Selected shRNA targeted mRNA sequences are common to both α - and β -Nrnx isoforms. The KD efficiency of each shRNA construct was quantified using a fluorescence assay described in the supplementary methods. shRNA sequences were combined into 2 Nrnx triple knockdown vectors (NrnxTKD1 and NrnxTKD2), each with unique shRNA sequences. The NrnxTKD1 construct encoded shRNAs for targets 5'-AATAGCCAAGCAACCATAATA-3', 5'-GTGTCCAAGTGATGATGAG-3', and 5'-CAGTCTCGGGAACAACACATA-3' for knockdown of Nrnx1, Nrnx2, and Nrnx3, respectively. The NrnxTKD2 construct contained shRNA sequences for the targets 5'-GGACAGATGACATCGCCATTG-3', 5'-GAACACAGATGACCTTCTG-3', and 5'-AAGTCTCGGAACTAGTAGAA-3' for knockdown of Nrnx1, Nrnx2, and Nrnx3, respectively. shRNA sequences were driven by either U6 or H1 promoters (see Fig. 1a).

cDNA constructs. To create the mGFP-Nrnx fusion constructs used for Western blotting, cDNAs for Nrnx-1 β (M96375), Nrnx-2 β (M96377, with amino acids 203–232 and 368–561 spliced out), and Nrnx-3 β (XM_008764732, with amino acids 202–231 spliced out and with nucleotides 968–979 from start ATG absent) were cloned in frame at the 3' end of the mGFP cDNA in a vector allowing for the expression of the construct from a CMV promoter. Nrnx-1 β Δ LNS was created by deleting the LNS domain of Nrnx-1 β using site-directed mutagenesis with the primers 5'-GGAATACGTCGTCGCCAGCGT-GTC-3' and 5'-GGAAGGCTGGTCGGTGAAGTGC-3'. This PCR removed amino acids 87–285 (UniProtKB - Q63373) and inserted a BspEI site in its place. pHluorin-Nrnx-1 β Δ LNS was created by inserting an AgeI, BspEI excised pHluorin cassette into the Nrnx-1 β Δ LNS BspEI site. Synaptophysin-EGFP and Synaptophysin-mCherry constructs were generated by fusing the ORF of synaptophysin (obtained via RT-PCR) in-frame to the 5' end of the

EGFP/mCherry cDNA contained in a pEGFP-C1-based expression vector. Synaptophysin-pHluorin (SypHl) has been previously described³⁸. LRRTM2-CFP was a gift from Dr. Ann Marie Craig. CMV promoters were used to drive the expression of all exogenous sensors and constructs.

Dissociated Hippocampal Cultures and Neuronal Transfection. Dissociated neuronal cultures were prepared from E18 embryonal Sprague Dawley rat hippocampi. All experiments on animals were approved by the Dalhousie University Committee on Laboratory Animals (UCLA Protocol #15–113) and performed in accordance with the approved guidelines. Cultures were grown in Neurobasal supplemented with B27 (ThermoFisher, Waltham MA). For all experiments, cultures of hippocampal neurons were transfected 10–14 days after plating using a calcium-phosphate precipitation protocol. Imaging experiments were conducted 3–4 days after transfection. For additional detail on culture and transfection experimental procedures please see ref. 38.

Immunocytochemistry and Western Blotting. Dissociated neuronal cultures were fixed with 4% paraformaldehyde at room temperature for 3 min followed by methanol at 4 °C for 10 minutes. Coverslips were washed with PBS, transferred onto parafilm wax, and blocked with 1% bovine serum albumin and 0.3% gelatin in PBS for 1 hr. Primary antibodies were diluted in blocking solution and applied for 24 hrs at room temperature. Primary antibodies include: Bassoon (Mouse monoclonal Ab, Enzo, SAP7F407, 1:400), Homer1 (Rabbit polyclonal Ab, Synaptic Systems, Lot # 160002, 1:3000), RIM1/2 (Rabbit polyclonal Ab, Synaptic Systems, Lot # 140203, 1:1000) and MAP2 (Guinea Pig polyclonal Ab, Synaptic Systems, Lot # 188004, 1:400). Coverslips were then washed with PBS and blocked for 30 minutes. Fluorescently labeled secondary antibodies were diluted in blocking solution and applied for 1 hr at room temperature. Secondary antibodies include: Alexa Fluor 660 (Goat anti-mouse, 1:1200), DyLight 549 (Donkey anti-rabbit 1:400), and AMCA (Donkey anti-guinea pig, Jackson Labs, 1:400). Coverslips were washed with PBS and mounted onto slides using Aqua-Mount (Thermo Scientific).

For western blotting, HEK 293 cells were transfected using polyethylenimine with 1 μ g mGFP-Nrxn-1 β , mGFP-Nrxn-2 β , or mGFP-Nrxn-3 β constructs and 10 μ g of either an empty knockdown plasmid, NrxnTKD1, or NrxnTKD2 per 35 mm dish. 10 μ g of lysed samples per lane were loaded on an 8% SDS-PAGE gel and then transferred to nitrocellulose membranes. Samples were blocked for 1 hour at room temperature with blocking solution (5% non-fat dry milk and 0.1% Tween-20 in TBS) and then incubated with primary antibodies overnight at 4 °C. Membranes were washed three times with 0.1% Tween-20 in TBS, blocked for 30 minutes and then incubated with HRP conjugated secondary antibodies for 1 hour at room temperature. HRP signals were detected using a chemiluminescence solution (Bio-Rad, Cat. # 170–5060). Primary antibodies used were anti-GFP (Rabbit polyclonal, Synaptic Systems, Cat # 132002, dilution of 1:5000) and anti-Tubulin (Mouse monoclonal, Sigma, 6-11B-1 at a dilution of 1:10,000). Secondary antibodies included Donkey Anti-Rabbit HRP (Jackson, 711-035-152, 1:10000) and Donkey Anti-Mouse HRP (Jackson, 715-035-150, 1:10000).

Characterization of pHl-Nrxn-1 β Δ LNS. Cultures of dissociated hippocampal neurons were transfected at 10–14 DIV with the pHl-Nrxn-1 β Δ LNS (pHl- Δ LNS) construct. After 3 days, cells were imaged on a Zeiss Observer 2.1 inverted microscope using a 63x objective, Photometrics Coolsnap HQ2 camera and SlideBook 6 imaging software. Image stacks of pHl- Δ LNS transfected axons were first acquired in pH 7.3 HBS buffer (described above). Neurons were then perfused with a pH 5.5 buffer (Composition in mM: 124 NaCl, 3 KCl, 10 MES, 5 D-glucose) for 5 minutes at which point a second image stack was acquired. Neurons were then re-perfused with the original pH 7.3 HBS buffer and a final image stack was acquired. Image stacks were converted to projected images according to maximum fluorescence and pHl- Δ LNS fluorescent puncta were segmented and measured using IPLab software.

Neuronal-COS7 Co-culture Assay. At 10 DIV, dissociated hippocampal neurons were transfected with 60 μ g of either an empty KD vector, NrxnTKD1, NrxnTKD2, or Nrxn-1 β Δ LNS per 60 mm dish along with 25 μ g Synaptophysin-mCherry (SypH-mCh) to label presynaptic specializations and serve as a measure for presynaptic clustering. Following transfection, coverslips were transferred to 12-well plates. The next day, COS7 cells were transfected using calcium phosphate precipitation with 30 μ g of CFP or LRRTM2-CFP per 35 mm well. After 24 hrs of expression, COS7 cells were trypsinized, pelleted, and re-suspended in conditioned neuronal media. COS7 cells were then seeded onto neurons at a density of approximately 10,000 cells per well of a 12-well plate. Co-cultures were maintained for 48 hours and then fixed and immunostained with anti-MAP2 to label neuronal dendrites. In regions where SypH-mCh expressing axons contacted transfected COS7 cells, image stacks of 2.8 μ m were acquired with a Zeiss Observer 2.1 inverted microscope using a 63x objective, Photometrics Coolsnap HQ2 camera and SlideBook 6 imaging software. Maximum projection images were created and exported for analysis. Images were analyzed for the number and intensity of SypH-mCh puncta per transfected COS7 cell using IPLab software. Contacts between SypH-mCh expressing axons and MAP2 positive dendrites were excluded from analysis. Images were acquired from 2 independent co-cultures.

Synaptophysin-pHluorin experiments. Cultures of hippocampal neurons were transfected with SypHl to quantify synaptic vesicle exocytosis as described³⁸. 80 μ g of either a control plasmid, NrxnTKD1, NrxnTKD2 or Nrxn-1 β Δ LNS were transfected along with 80 μ g of SypHl. The presynaptic marker SypH-mCh was also included in the transfection to identify transfected axons. Fluorescence microscopy was carried out on a Nikon TE2000 epifluorescence microscope equipped with a 60x (N.A. 1.40) objective, Smart shutter (Sutter Instruments) and Lumencor solid-state illumination. Images were acquired at 10 Hz with a Hamamatsu ORCA CCD camera and IPLab software. Experiments were performed at 36 \pm 2 °C in HBS solution containing (in mM) 110 NaCl, 5.3 KCl, 2 CaCl₂, 1 MgCl₂, 20 4-(2-hydroxyethyl)-1-piperazineethanesulfonic acid (HEPES), and 25 D-glucose adjusted to pH 7.30, supplemented with 10 μ M 6,7-dinitroquinoxaline-2,3-dione (DNQX) and 50 μ M (2R)-amino-5-phosphonovaleric acid (APV) to prevent recurrent excitation. Axons

were selected based on Syph-mCh fluorescence, and SyphH1 fluorescence changes were measured in response to field stimulation employing 1 ms square current pulses yielding electrical fields of approximately 10 V/cm through platinum electrodes placed 0.5 cm apart. Image acquisition and extracellular stimulation were synchronized using a Master-8 stimulator (AMPI). Stimulus trains of 80 stimuli at 80 Hz were given to measure the readily releasable pool of synaptic vesicles. In this study, we chose a higher stimulus number and stimulation frequency to deplete the RRP than in earlier studies by us and others^{38,41,42} to maximize mobilization of readily releasable vesicles while minimizing contributions of RRP refilling to the signal. Fluorescence increases in response to isolated stimuli (100 trials at 0.2 Hz) provided a relative measure of release probability (Pr) at individual presynaptic specializations. Images were acquired from at least two individual hippocampal cultures. Subsequent image analysis was performed using IPLab software. Image stacks were background-subtracted and aligned. For SyphH1 RRP and Pr, experiments, synaptic regions for measurement were identified according to an RRP threshold. Synaptic regions of measurement had a size between 0.32 and 0.64 μm^2 . Multi-trial fluorescent responses at each synapse were averaged and an average synaptic response for each experiment was calculated. Data were expressed as change in fluorescence (ΔF). The statistical significance ΔF values for Ctrl, NrnxTKD1, and Nrnx-1 β Δ LNS groups was tested with a one-way ANOVA and post hoc Tukey tests.

Assessment of active zone size and synaptic density. To assess the effect of Nrnx disruption on active zone size and synaptic density, we performed immunocytochemistry on cultures of transfected hippocampal neurons. Neurons were transfected with three cDNA plasmids: 1) either TKD1, TKD2, Nrnx-1 β Δ LNS, or control plasmid, 2) synaptophysin-EGFP (syph-EGFP), a fusion protein that labels clusters of synaptic vesicles and 3) cytosolic EGFP, as an axonal fill stain. Three days after transfection, neurons were immunostained for Bsn, RIM1/2 and MAP2 to assess active zone size and for Bsn, Homer1 and MAP2 to quantify synaptic density. Experimenters were blinded to the experimental conditions during image acquisition and analysis. Fluorescence images were taken on a Nikon TE2000 epifluorescence microscope equipped with a 60 X (N.A. 1.40) objective and Hamamatsu camera (Model C4742-80-12AG). To quantify the effect of Nrnx disruption on the size of active zone cytomatrices, we measured the fluorescence intensity of Bsn and RIM1/2 puncta (segment size = 0.5 μm^2) that co-localized with syph-EGFP + EGFP expressing axons and MAP2 positive dendrites. Group averages of Bsn and RIM1/2 fluorescence were compared using either a one-way analysis of variance (ANOVA, for Ctrl, TKD1, TKD2) or a two-tailed Student's t-test for independent samples (for Ctrl and Nrnx-1 β Δ LNS).

To quantify the effect of Nrnx disruption on synaptic density, we identified points at which axons of transfected neurons traversed MAP2-positive dendrites. We then determined the fraction of contact points bearing co-localized Bsn and Homer1 puncta as a measure of the density of synaptic contacts made by the transfected presynaptic neuron. An intensity threshold was set for both Homer1 and Bsn and kept constant for each experiment for a given transfected neuronal culture. Axodendritic contacts with both Homer1 and Bsn puncta intensities above threshold were scored as synaptic and contacts that failed these criteria were scored non-synaptic. Averages of the percentage of synaptic axodendritic contacts in each transfected culture were compared between groups using a one-way analysis of variance (ANOVA). Fasciculated neurites were excluded from analysis. Images were acquired from at least 2 separate hippocampal cultures.

Quantification of synapse formation and elimination. To assess the effect of Nrnx perturbation on the stability of synaptic connections, we expressed fluorescently labeled pre- and postsynaptic proteins in hippocampal neurons and quantified the number of stable, newly formed and eliminated synapses over 24 hours. The presynaptic marker, synaptophysin-mCherry (Syph-mCh), was co-transfected with either a control plasmid, NrnxTKD1, or Nrnx-1 β Δ LNS at 13 day *in vivo* (DIV). In a second transfection at 15 DIV, PSD95-EGFP was introduced to label the postsynaptic densities in a separate population of neurons. On the following day, referred to in figures as day 0 (D0), coverslips were transferred to an imaging chamber, perfused with HBS solution at 36 ± 2 °C, and imaged with a Zeiss Observer 2.1 inverted microscope using a 63x objective, Photometrics Coolsnap HQ2 camera and SlideBook 6 imaging software. Stacks comprising 12 images over a distance of 3.85 μm were acquired for experiments that showed Syph-mCh positive axons in contact with PSD95-EGFP positive dendrites. The XY coordinates of each experiment were recorded and coverslips were returned to the incubator. The following day, a second image stack was acquired for each experiment (D1). Image stacks were converted to a maximum intensity projected image and exported for analysis. D0 and D1 images were first analyzed individually to detect synaptic contacts between Syph-mCh positive axons and PSD95-EGFP positive dendrites in control, NrnxTKD1, and Nrnx-1 β Δ LNS groups. The co-localization of a Syph-mCh punctum and a PSD95-EGFP punctum was scored a synapse if the center-to-center distance between both puncta was less than 0.8 μm . Next, the corresponding D1 image was aligned to the D0 image and the number of stable, newly formed, and eliminated synapse was quantified. Analysis was performed using IPLab software. Experiments with NrnxTKD1 construct and the Nrnx-1 β Δ LNS construct were performed independently. Using a Student's t-test for independent samples, the percentage of stable, newly formed, and eliminated synapses were compared between NrnxTKD1, Nrnx-1 β Δ LNS and the respective control groups. Images were acquired from 6 separate hippocampal cultures for NrnxTKD1 experiments and 2 separate hippocampal cultures for Nrnx-1 β Δ LNS experiments.

References

1. Purves, D. & Lichtman, J. W. Elimination of synapses in the developing nervous system. *Science* **210**, 153–157 (1980).
2. Goda, Y. & Davis, G. W. Mechanisms of synapse assembly and disassembly. *Neuron* **40**, 243–264 (2003).
3. Okawa, H. *et al.* Illuminating the multifaceted roles of neurotransmission in shaping neuronal circuitry. *Neuron* **83**, 1303–1318 (2014).
4. Siddiqui, T. J. & Craig, A. M. Synaptic organizing complexes. *Curr Opin Neurobiol.* **21**, 132–143 (2011).
5. Krueger, D. D., Tuffy, L. P., Papadopoulos, T. & Brose, N. The role of neurexins and neuroligins in the formation, maturation, and function of vertebrate synapses. *Curr Opin Neurobiol.* **22**, 412–422 (2012).

6. Um, J. W. & Ko, J. LAR-RPTPs: synaptic adhesion molecules that shape synapse development. *Trends Cell Bio.* **23**, 465–475 (2013).
7. Takahashi, H. & Craig, A. M. Protein tyrosine phosphatases PTP δ , PTP σ , and LAR: presynaptic hubs for synapse organization. *Trends Neurosci.* **36**, 522–534 (2013).
8. Bembem, M. A., Shipman, S. L., Nicoll, R. A. & Roche, K. W. The cellular and molecular landscape of neuroligins. *Trends Neurosci.* **38**, 496–505 (2015).
9. Jamain, S. *et al.* Mutations of the X-linked genes encoding neuroligins NLGN3 and NLGN4 are associated with autism. *Nat. Genet.* **34**, 27–29 (2003).
10. Francks, C. *et al.* LRRTM1 on chromosome 2p12 is a maternally suppressed gene that is associated paternally with handedness and schizophrenia. *Mol. Psychiatry.* **12**, 1129–1139 (2007).
11. Piton, A. *et al.* Mutations in the calcium-related gene IL1RAPL1 are associated with autism. *Hum. Mol. Genet.* **17**, 3965–3974 (2008).
12. Pinto, D. *et al.* Functional impact of global rare copy number variation in autism spectrum disorders. *Nature* **466**, 368–372 (2010).
13. Gauthier, J. *et al.* Truncating mutations in NRXN2 and NRXN1 in autism spectrum disorders and schizophrenia. *Hum. Genet.* **130**, 563–573 (2011).
14. Vaags, A. K. *et al.* Rare deletions at the neurexin 3 locus in autism spectrum disorder. *Am. J. Hum. Genet.* **90**, 133–141 (2012).
15. Ichtchenko, K. *et al.* Neuroligin 1: a splice site-specific ligand for beta-neurexins. *Cell* **81**, 435–443 (2011).
16. Linhoff, M. W. *et al.* An unbiased expression screen for synaptogenic proteins identifies the LRRTM protein family as synaptic organizers. *Neuron* **61**, 734–749 (2009).
17. Ko, J., Fuccillo, M. V., Malenka, R. C. & Südhof, T. C. LRRTM2 functions as a neurexin ligand in promoting excitatory synapse formation. *Neuron* **64**, 791–798 (2009).
18. Uemura, T. *et al.* Trans-synaptic interaction of GluRdelta2 and neurexin through Cbln1 mediates synapse formation in the cerebellum. *Cell* **141**, 1068–1079 (2010).
19. Pettem, K. L. *et al.* The Specific alpha-neurexin interactor calyntenin-3 promotes excitatory and inhibitory synapse development. *Neuron* **80**, 113–128 (2013).
20. Ushkaryov, Y. A., Petrenko, A. G., Geppert, M. & Südhof, T. C. Neurexins: synaptic cell surface proteins related to the alpha-latrotoxin receptor and laminin. *Science* **257**, 50–56 (1992).
21. Siddiqui, T. J., Pancaroglu, R., Kang, Y., Rooyakkers, A. & Craig, A. M. LRRTMs and neuroligins bind neurexin with a differential code to cooperate in glutamate synapse development. *J. Neurosci.* **30**, 7495–7506 (2010).
22. Graf, E. R., Zhang, X., Jin, S.-X., Linhoff, M. W. & Craig, A. M. Neurexins induce differentiation of GABA and glutamate postsynaptic specializations via neuroligins. *Cell* **119**, 1013–1026 (2004).
23. Scheiffele, P., Fan, J., Choih, J., Fetter, R. & Serafini, T. Neuroligin expressed in nonneuronal cells triggers presynaptic development in contacting axons. *Cell* **101**, 657–669 (2000).
24. Missler, M. *et al.* (2003) Alpha-neurexins couple Ca²⁺ channels to synaptic vesicle exocytosis. *Nature* **423**, 939–948 (2000).
25. Anderson, G. R. *et al.* Beta-neurexins control neural circuits by regulating synaptic endocannabinoid signaling. *Cell* **162**, 1–14 (2015).
26. Varoqueaux, F. *et al.* Neuroligins determine synapse maturation and function. *Neuron* **51**, 741–754 (2006).
27. Soler-Llavina, G. J., Fuccillo, M. V., Ko, J., Südhof, T. C. & Malenka, R. C. The neurexin ligands, neuroligins and leucine-rich repeat transmembrane proteins, perform convergent and divergent synaptic functions *in vivo*. *Proc. Natl. Acad. Sci. USA* **108**, 16502–16509 (2011).
28. Ko, J., Soler-Llavina, G. J., Fuccillo, M. V., Malenka, R. C. & Südhof, T. C. Neuroligins/LRRTMs prevent activity- and Ca²⁺/calmodulin-dependent synapse elimination in cultured neurons. *J. Cell Bio.* **194**, 323–334 (2011).
29. Ullrich, B., Ushkaryov, Y. A. & Südhof, T. C. Cartography of neurexins: more than 1000 isoforms generated by alternative splicing and expressed in distinct subsets of neurons. *Neuron* **14**, 497–507 (1995).
30. Laurén, J., Airaksinen, M. S., Saarma, M. & Timmusk, T. Ö. A novel gene family encoding leucine-rich repeat transmembrane proteins differentially expressed in the nervous system. *Genomics* **81**, 411–421 (2003).
31. Fuccillo, M. V. *et al.* Single-cell mRNA profiling reveals cell-type-specific expression of neurexin isoforms. *Neuron* **87**, 326–340 (2015).
32. de Wit, J. *et al.* LRRTM2 interacts with Neurexin1 and regulates excitatory synapse formation. *Neuron* **64**, 799–806 (2009).
33. Hata, Y., Butz, S. & Südhof, T. C. CASK: A novel dlg/PSD95 homolog with an N-terminal calmodulin-dependent protein kinase domain identified by interaction with neurexins. *J. Neurosci.* **16**, 2488–2494 (1996).
34. Butz, S., Okamoto, M. & Südhof, T. C. A tripartite protein complex with the potential to couple synaptic vesicle exocytosis to cell adhesion in brain. *Cell* **94**, 773–782 (1998).
35. Blundell, J. *et al.* Neuroligin-1 deletion results in impaired spatial memory and increased repetitive behavior. *J. Neurosci.* **30**, 2115–2129 (2010).
36. Zhang, B. *et al.* Neuroligins sculpt cerebellar purkinje-cell circuits by differential control of distinct classes of synapses. *Neuron* **87**, 781–796 (2015).
37. Futai, K. *et al.* Retrograde modulation of presynaptic release probability through signaling mediated by PSD-95–neuroligin. *Nat. Neurosci.* **10**, 186–195 (2007).
38. Matz, J., Gilyan, A., Kolar, A., McCarvill, T. & Krueger, S. R. Rapid structural alterations of the active zone lead to sustained changes in neurotransmitter release. *Proc. Natl. Acad. Sci. USA* **107**, 8836–8841 (2010).
39. Holderith, N. *et al.* Release probability of hippocampal glutamatergic terminals scales with the size of the active zone. *Nat. Neurosci.* **15**, 988–997 (2012).
40. Chubykin, A. A. *et al.* Activity-dependent validation of excitatory versus inhibitory synapses by neuroligin-1 versus neuroligin-2. *Neuron* **54**, 919–931 (2007).
41. Pyle, J. L., Kavalali, E. T., Piedras-Renteria, E. S. & Tsien, R. W. Rapid reuse of readily releasable pool vesicles at hippocampal synapses. *Neuron* **28**, 221–231 (2000).
42. Murthy, V. N., Schikorski, T., Stevens, C. F. & Zhu, Y. Inactivity produces increases in neurotransmitter release and synapse size. *Neuron* **32**, 673–682 (2001).

Acknowledgements

Funded by Natural Sciences and Engineering Research Council of Canada (NSERC) Discovery Grant (#326821). We thank Dr. Ann Marie Craig for sharing the LRRTM2-CFP construct.

Author Contributions

S.R.K. designed and coordinated experiments and assisted with data acquisition and analysis for figure 2. D.P.Q. performed the majority of data acquisition and analysis. S.R.K. and D.P.Q. wrote the paper. R.N.G. and H.A. performed experiments and analyzed data involved with figures 2 and 4. M.W. and J.P.F. helped with article revisions. A.K. provided hippocampal cultures and helped with article revisions.

Additional Information

Supplementary information accompanies this paper at <http://www.nature.com/srep>

Competing financial interests: The authors declare no competing financial interests.

How to cite this article: Quinn, D. P. *et al.* Pan-neurexin perturbation results in compromised synapse stability and a reduction in readily releasable synaptic vesicle pool size. *Sci. Rep.* 7, 42920; doi: 10.1038/srep42920 (2017).

Publisher's note: Springer Nature remains neutral with regard to jurisdictional claims in published maps and institutional affiliations.



This work is licensed under a Creative Commons Attribution 4.0 International License. The images or other third party material in this article are included in the article's Creative Commons license, unless indicated otherwise in the credit line; if the material is not included under the Creative Commons license, users will need to obtain permission from the license holder to reproduce the material. To view a copy of this license, visit <http://creativecommons.org/licenses/by/4.0/>

© The Author(s) 2017